Int. J. Electrochem. Sci., 14 **(2019)** 6790 – 6813, doi: 10.20964/2019.07.51

International Journal of
ELECTROCHEMICAL
SCIENCE
www.electrochemsci.org

Investigation of Influence of Surface Roughness on Pitting Corrosion of Duplex Stainless Steel 2205 using Various Electrochemical Techniques

Yiwei Tang, Nianwei Dai, Jun Wu, Yiming Jiang, Jin Li *

Department of Material Science, Fudan University, Shanghai, China
*E-mail: corrosion@fudan.edu.cn

Received: 8 March 2019 / *Accepted:* 26 April 2019 / *Published:* 10 June 2019

The metastable and stable pitting behaviors on different surface roughness finishes for DSS 2205 stainless steel have been investigated. Surface roughness was analyzed through the adoption of atomic force microscopy (AFM). Pitting corrosion susceptibility of duplex stainless steel (DSS) 2205 in sodium chloride solution was evaluated by means of critical pitting temperature (CPT), potentiodynamic polarization, electrochemical impedance spectroscopy (EIS) and potentiostatic measurement. The statistical analysis revealed that the smoother surface of DSS 2205 exhibited lower pitting corrosion susceptibility and better corrosion resistance. Based on the surface analysis, depth-width ratio was introduced as a parameter to present surface roughness and was used in the characterization of the relationship between surface roughness and pitting corrosion.

Keywords: Pitting corrosion, Surface roughness, Electrochemical technique, Duplex stainless steel, Depth-width ratio

1. INTRODUCTION

Duplex stainless steel (DSS) has been widely used in oil and gas exploration as well as in marine environments, due to its good corrosion resistance in highly aggressive environments, especially in the circumstances containing chloride ions. Because of its practical importance, the pitting corrosion resistance of DSS, which is closely related to the service conditions, has been extensively studied.

Among the factors that affect the pitting corrosion resistance of stainless steels, surface roughness, which is controlled by different surface treatments, is believed to be a critical parameter. Previous researches have mentioned the relationship between surface roughness and typical pitting corrosion parameters including pitting potential [1] and critical pitting temperature [2,3] (CPT). Pitting potential, which is the minimum potential of stable pitting propagation, was found to be much lower on

rougher surface. The results for CPT also indicated that rough surface led to greater susceptibility to pitting. A theoretical model was established by Moayed et al. [2] to illustrate the relation between surface roughness and critical pitting temperature (CPT). Then Hong and Nagumo [4] focused on the influence of surface roughness on metastable pitting, which is considered as the precursor of stable pitting, and found out that it was more harder for metastable pits to occur on smooth surface in the early stage of corrosion. Moreover, it was reported that metastable pitting nucleation [5] and its propagation process to stable pitting [6] was strongly dependent on surface geometry, which could control the diffusion rate and maintain the aggressive environment within the pit site. To verify this hypothesis, electrochemical noise (EN) was also adopted to monitor the pitting corrosion behavior before reaching the critical condition, and to evaluate the pitting probability of stainless steel [7,8].

However, few works have combined these parameters or methods, and a simple, reliable form to express the influence of surface roughness on pitting corrosion resistance is required. Moreover, a theoretical model has not been established between surface roughness and pitting susceptibility in the field of DSS, which has more complicated phase composition than austenitic SS. In the present work, we have focused on the effects of surface roughness on the metastable and stable pitting initiation of DSS and the different techniques to detect them. The proper parameters to describe the interrelation between roughness situation and pitting initiation has been measured as well.

2. MATERIALS AND SAMPLE PREPARATION

The material used in the work was commercial 2205 duplex stainless steel (DSS2205). Its chemical composition is listed in Table 1. All the specimens were stabilized through solid solution heat treatment (at 1050 ºC for 1h followed by water quenching). The specimens were sealed in epoxy resin in order to ensure the exposure area was 10 mm × 10 mm. The reverse side of the specimen was welded to a copper wire to provide an electrical connection. The surfaces of the specimens were prepared by mechanical grinding (180 #, 600 #, 1000 # and 2000 #) and then polished using diamond polishing paste with particles of 2.5 μm in order to produce the same initial surface condition. The final surface roughness of the specimens was carried out using different grits abrasive paper. Before each experiment, the specimens were degreased by ethanol, rinsed by distilled water and dried in an oven for at least 4 hours.

Table 1. The chemical composition (wt.%) of DSS 2205

Element	C	Si	Mn	P	S	Cr	Mo	Ni	N	Cu	Fe
wt.%	≤0.025	≤0.05	≤1.50	≤0.025	0.001	22.00～23.00	3.00～3.20	5.51	0.16	0.15	Bal.

2.2. Morphological characterization

The surface morphology was observed and analyzed with optical microscope, step profiler and dimension icon atomic force microscope (AFM; Bruker, Germany). The pit morphology was studied by optical microscope and scanning electron microscopy (SEM; PHILIPS XL30FEG, Netherlands)

2.3. Electrochemical evaluation

The electrochemical test methods used to evaluate the pitting corrosion susceptibility of specimens were as follows: measurements of critical pitting temperature, potentiodynamic polarization, electrochemical impedance spectroscopy, electrochemical noise test and potentiostatic test. All these electrochemical measurements were performed in the 1 M sodium chloride aqueous solution using a PARSTAT™ MC multi-channel potentiostat/galvanostat. The reference electrode was the saturated calomel electrode (SCE).

2.3.1. Critical pitting temperature (CPT)

Before the CPT measurement, the cathodic polarization of the working electrode was firstly performed at -900 mV_{SCE} for 120 s and was then stabilized at open circuit potential (OCP) for 10 min at 5 ºC. CPT measurement was conducted at an applied potential of 750 mV_{SCE} with the solution temperature rising from 20 ºC at the heating rate of 1ºC·min^{-1}. The current density was recorded simultaneously along with the temperature data. The CPT of the specimen was determined as the temperature when current density exceeded 100 μA·cm^{-2}. After the current reach the threshold of 1 mA·cm^{-2}, the solution was cooled down at a rate of 2 ºC·min^{-1}. The pitting repassivation temperature (PRT) was determined as the temperature when the current went below to 100 μA·cm^{-2} in the reverse scan.

2.3.2. Potentiodynamic Polarization

The potentiodynamic polarization was conducted within the temperature range from 45ºC to 60 ºC at a scan rate of 10 mV/min. Before the polarization measurement, the specimen went through cathodic polarization and OCP stabilization as well. The polarization potential range was from -100 mV to 1200 mV vs. OCP.

2.3.3. Electrochemical impedance spectroscopy (EIS)

The potential applied in the experiment was 500 mV_{SCE}. The testing temperature range was determined by CPT measurement. The EIS in the frequency range from 10 kHz to 1 MHz was measured with a perturbation signal of 10 mV and 12 points per decade. The solution temperature was selected based on CPT measurement.

2.3.4. Potentiostatic Measurement

The potentiostatic electrochemical test was performed within a temperature range from 50 ºC to 60 ºC. The potential applied in the test was 200 mV_{SCE}, according to the results of potentiodynamic

polarization curves. The current transient which exceeded 500 nA above the background passive current was recorded.

3. RESULTS AND DISCUSSION

3.1. Surface morphology and roughness

The AFM images of DSS2205 surface morphologies prepared by abrasive papers of different grit numbers are displayed in Fig. 1. According to the images, surface roughness decreases with the increase of grit number. For each specimen, a series of profile line-scans were conducted, and the corresponding average roughness value was calculated. Fig. 2 shows the typical surface profiles of different surface roughness conditions obtained from AFM roughness analysis. It can be clearly observed from the Fig. 2 that the grinding process with large particle abrasive paper (180#) produced open and deep grooves on the surface, and the peak height and valley depth of the surface topography decreased significantly with the increasing of grit number. The average surface roughness (R_a) was commonly used to represent the arithmetical mean deviation of the roughness profile of the surface and the values were compared in Table 2. The values of R_a in the table illustrate that the surface roughness of the prepared specimens span over two orders of magnitude.

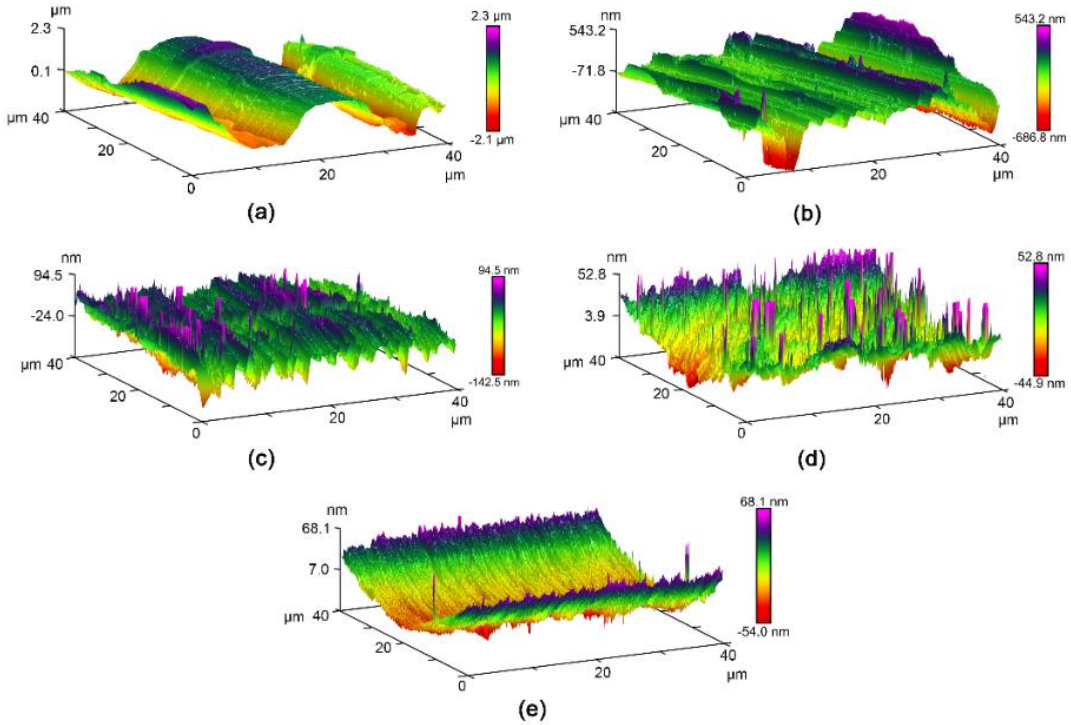

Figure 1. AFM images of DSS2205 surface morphologies prepared using abrasive papers of different grits: a) 180 #, b) 600 #, c) 1000 #, d) 2000 # and e) polished by particles of 2.5μm. All the corresponding length bar is denoted on each image respectively.

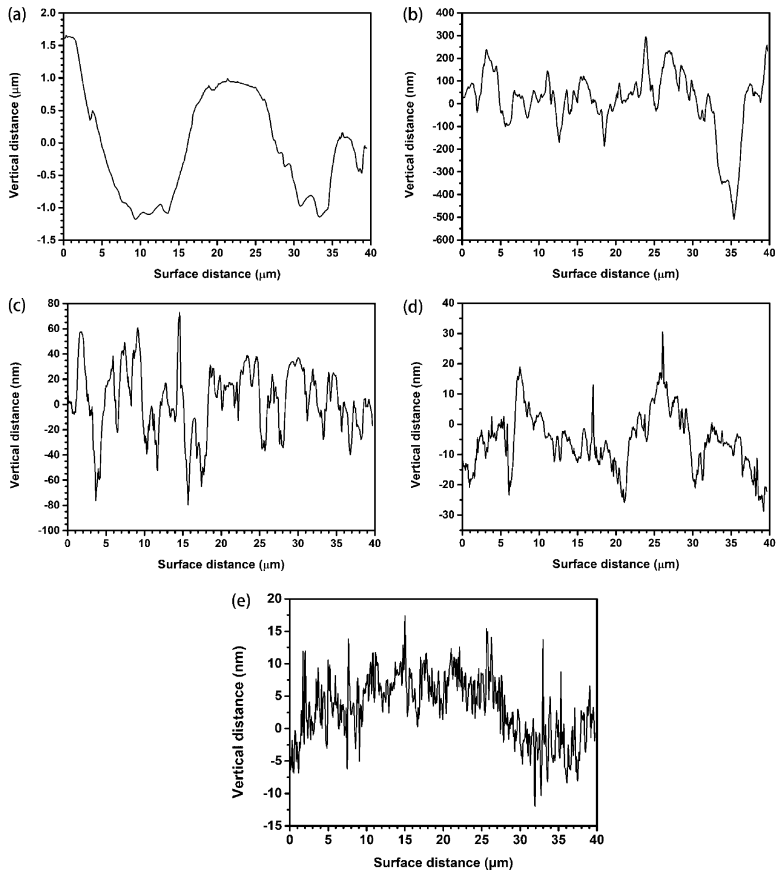

Figure 2. Typical surface profiles of different surface finished conditions: a) 180 #, b) 600 #, c) 1000 #, d) 2000 # and e) polished by particles of 2.5μm

Table 2. Average surface roughness of DSS2205 specimens prepared using different measurements

Surface measurements	Mechanical grinding				Polishing	
	180#	600#	1000#	2000#		
Average surface roughness R_a (nm)	526 ± 70	134 ± 32	20 ± 2	7 ± 2	2	± 1

3.2. Surface effects on critical pitting temperature

Critical pitting temperature (CPT) can be used as a means for ranking susceptibility to pitting corrosion [9]. Therefore, this parameter was measured preliminarily to confirm the disparity of pitting resistance of the specimens with different surface conditions. Fig. 3 shows the current-temperature output of the working electrodes in the CPT method. The CPT value for each surface roughness sample was repeated at least three times, and the mean values and deviations of CPT for different surface finishes are shown in Table 3 and Fig. 4. It is obvious that the CPT values increases as the surface roughness decreases. For the roughest surface (ground with 180 # abrasive paper), the CPT value was 50 ºC, about 10 ºC lower than the value of the polished surface. The result reveals the remarkable effect of surface roughness on duplex stainless steels. Moreover, same variation trend with surface roughness was found

in the deviations of CPT. According to the results compared in Table 3, the standard deviation of smoothest surface finish (2.5 μm paste) was within a range of 1.63 ºC whilst that of 180 # had a range of almost 3 ºC. It can be concluded that the reproducibility of CPT on the smoother surface is distinctly higher than on the rougher one.

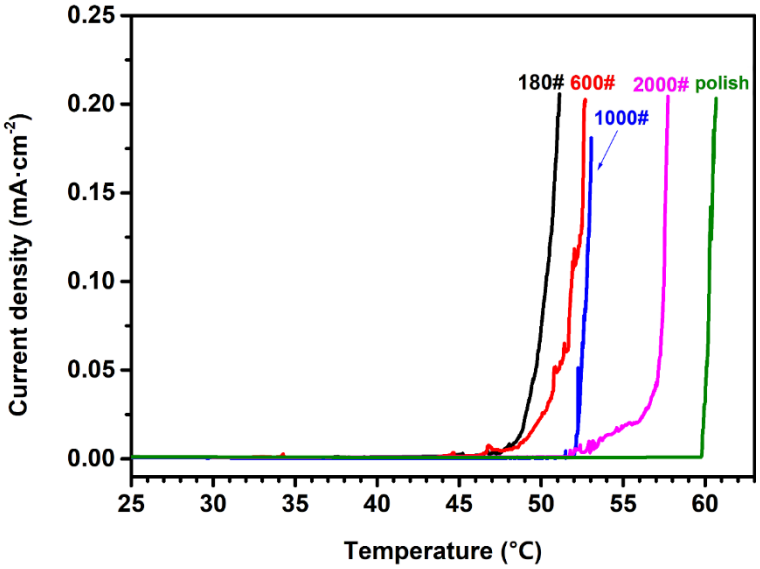

Figure 3. Current–temperature curves obtained from CPT method on DSS2205 at 0.75 V (SCE) in 1 M NaCl.

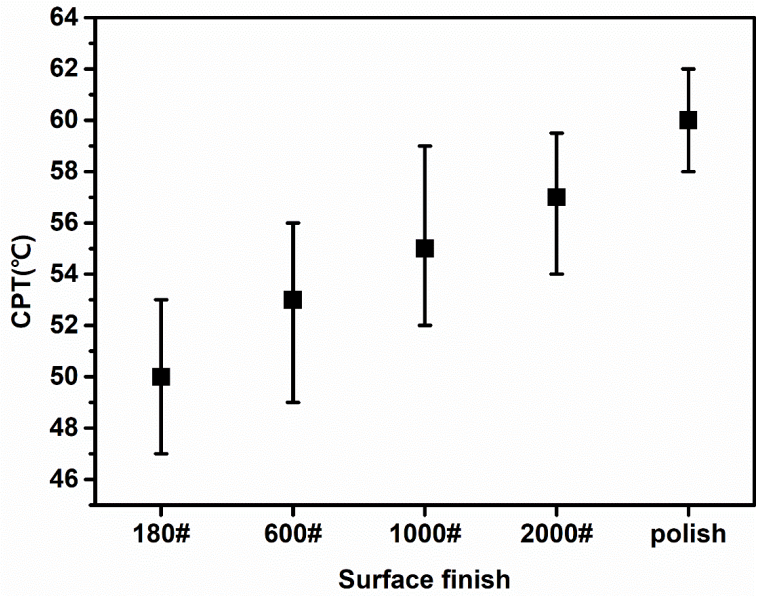

Figure 4. Mean values and deviations of the CPT on various surface finish samples for DSS2205

This result is in accordance with the model of CPT transition proposed by Salinas-Bravo and Newman **[10]**. In their work, the CPT is defined as the temperature when the i_{crit} is equal to the i_{limit} According to the model, a critical current density of passivation (i_{crit}) exists in the concentrated solution

inside pit, which increases with temperature more rapidly than the diffusion-limited anodic current density (i_{limit}). In addition, i_{crit} is independent of the pit morphology while i_{limit} is not.

Table 3. Mean values and standard deviations of CPT of DSS2205 specimens with different surface roughness

Surface finish	Average CPT (℃)	Std. dev. (℃)
180#	50	2.95
600#	53	2.87
1000#	55	2.65
2000#	57	2.25
2.5μm polished	60	1.63

Therefore, the effective diffusion length of the pit and the distribution of the initial pit sizes and shapes would lead to the variation and deviation of i_{limit}. These changes of i_{limit} are finally reflected in the change of CPT values. The schematic diagram of this model is shown in Fig. 5. In this measurement, the pitting nucleation area distributed much more widely across the rougher surface, and also had a broader distribution of shapes and sizes, which leads to the larger deviation of CPT, as show in Fig. 5. Moreover, narrow deep grooves on rougher surface increased the effective diffusion length of the pitting area, so making the concentrated local solution environment easier to maintain, and that reduced i_{limit} as well as CPT values.

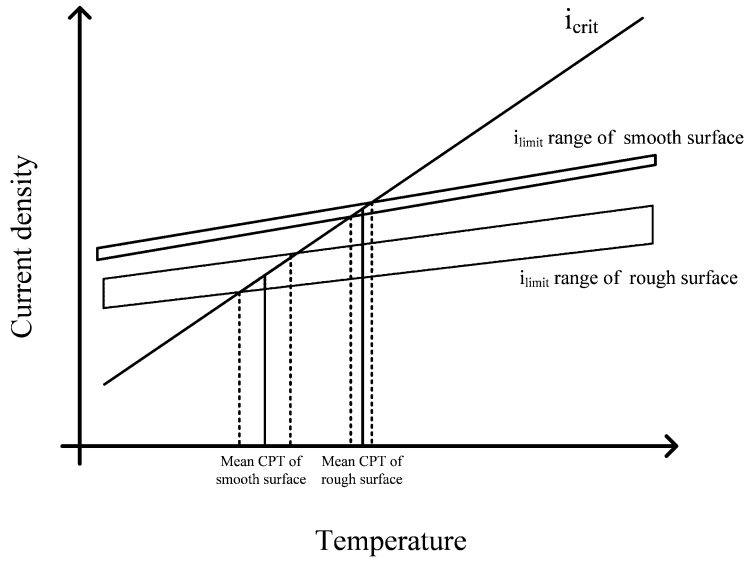

Figure 5. Schematic diagram of the i_{limit} and i_{crit} vs. temperature on different surface roughness conditions

Pitting repassivation temperature (PRT) measurement was also carried out. PRT represents the pitting repassivation capability of stainless steel because pitting corrosion has been proved to be

thermally irreversible **[11]**. In this research, PRT can reveal the influence of surface roughness on stable pit propagation and repassivation **[12]**. Fig. 6 depicts the typical cyclic temperature-changing measurement curve of DSS2205. From the results, it was observed that the current density did not decrease instantly once the temperature dropped, suggesting that pitting corrosion of DSS2205 still remained in the propagation stage. The rapid drop of the current density after peak value indicated the occurrence of repassivation behavior and the results are summarized in Table 4. The values of PRT for the specimens were in the range from 35 ºC to 37 ºC, and the standard deviations were close as well, within 1.2 ºC. Unlike the CPT values, there is no obvious disparity between them. Fig. 6 also shows that the maximum current density was independent of surface roughness, indicating that surface morphology might not be a controlling factor in the propagation stage and possible repassivation process of pitting corrosion. Based on the results above, the effects of surface roughness on pitting corrosion are mainly concerned in the nucleation of pitting and the conversion from metastable to stable pitting.

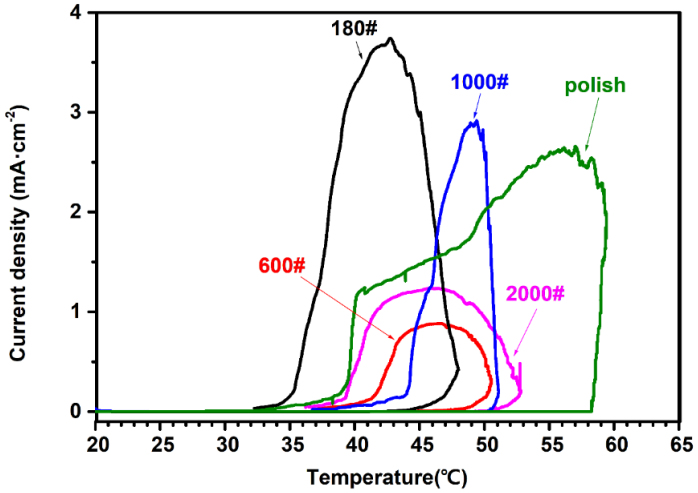

Figure 6. Current-temperature curve obtained from PRT measurement on DSS2205 at 0.75 V (SCE) in 1 M NaCl

Table 4. Mean values and standard deviations of CPT of DSS2205 specimens with different surface roughness

Surface finish	Average PRT(℃)	Standard deviation (℃)
180#	34	1.15
600#	36	0.74
1000#	37	0.66
2000#	35	0.86
2.5μm polished	36	1.09

3.3. Surface effects on potentiodynamic polarization

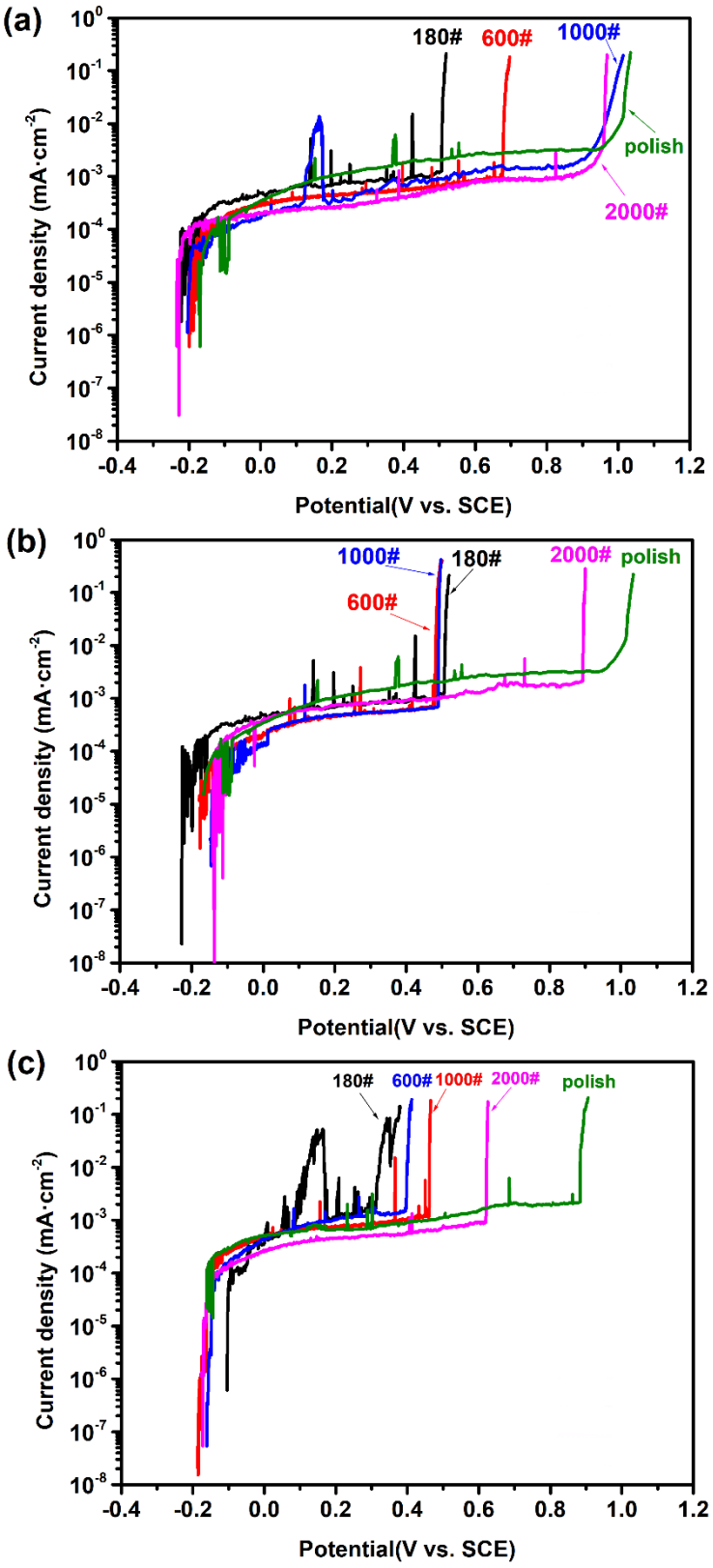

Figure 7. Potentiodynamic polarization curve of DSS2205 with different surface roughness in 1 M NaCl at different temperatures: (a) 50 ºC; (b) 55 ºC and (c) 60 ºC

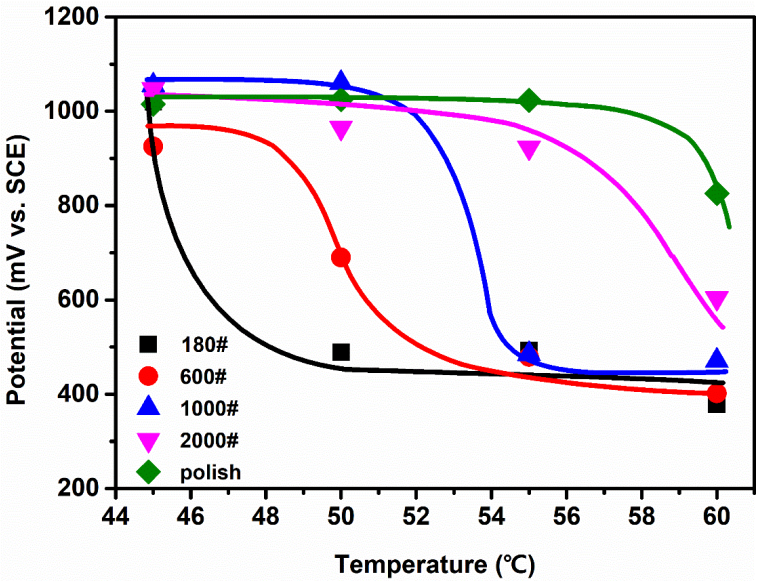

Figure 8. Breakdown potentials as a function of temperature for DSS2205 with different surface roughness in 1 M NaCl

Potentiodynamic polarization is another common method to evaluate the pitting corrosion resistance of SS through measuring the breakdown potential (E_b), which is the potential where current density exceeds 100 μA·cm^{-2} as determined by Qvarfort [13]. Fig. 7(a) shows the typical potentiodynamic polarization curve of DSS2205 with different surface roughness degrees in 1 M sodium chloride solution at 50 ºC. The polarization results for specimens at 55 ºC and 60 ºC are displayed in Fig. 7(b) and Fig. 7(c), respectively. Obviously, E_b shifted in positive direction as the surface became smooth at all temperature conditions. For instance, at 50 ºC, E_b values increased from 500 mV for the 180# surface finish, to 1100 mV for the 2.5 μm paste finish. A similar increase was also observed at 50 ºC and 60 ºC, which was from 450 mV to 1100 mV and from 400 mV to 900 mV respectively. E_b values are plotted as a function of temperature in Fig. 8 based on the experiments measured from 45 ºC to 60 ºC, CPT could also be defined as the temperature where the potential declined sharply to breakdown potential range [2]. The results were consistent with those obtained from the potentiostatic CPT measurement, suggesting a rougher surface promoted the occurrence of stable pitting. Since the rougher surface was considered to contain more narrow-mouth cavities, which had a higher possibility to precipitate a salt film on the pit surface, the local saturated environment inside the pit was more easily maintained and the pit stability was enhanced. As a result, the requirement for salt film formation was less on the coarse surface. The formation rate of salt film is demonstrated to be reduced with the decrease of modal current density of the metastable pit, which corresponds to a lower potential [6]. It is therefore reasonably to deduce that the potential of metastable-stable pit transition declines on a coarse surface.

Moreover, some current transient can be seen in the passive domain of the polarization curve. These current peaks represented the metastable pitting activity below E_b. For further study, all the current transients which were 1 μA larger than the background passive current density had been recorded. Fig. 7 (a), (b) and (c) indicate that the potential where current peaks first appeared increased as the surface became smoother. At 50 ºC, the initial occurrence of a transient was around 150 to 250 mV (SCE) for the relatively rough 180# surface, and for the smoother polished surface the potential was above 400 mV

(SCE). For the rest of the specimens of 600#, 1000# and 2000#, the potential was in the range from 200 mV (SCE) to 400 mV (SCE). When the temperature went to 60 ºC, the mean value of the potential for the specimen with a polished surface was still about 100 mV above that of the rougher surface one, based on the results obtained from the repeated experiment for each sample. In addition, the number of the transients also showed a growth trend as surface roughness increased. According to AFM results, rougher surface provides a larger number of more occluded sites which can easily form the diffusion barrier and establish a concentration gradient [14]. The metastable pit was demonstrated to occur at the pre-existed occluded site which can maintain the internal solution concentration [15], so these results illustrate that the rougher surface enhances the possibility of metastable pit nucleation and can activate metastable pits at lower potential. Consequently, these current transients prove the influence of surface roughness on the initiation of pitting corrosion.

3.4. Surface effect on electrochemical impedance spectroscopy (EIS)

In order to ensure whether the influence of surface roughness on pitting corrosion was generated from passive film resistance change or not, EIS measurement was applied. The solution temperatures were 45 ºC and 50 ºC, which were slightly lower than the CPT based on the aforementioned electrochemical measurements. Fig. 9(a) shows the EIS results of different surface roughness under applied potential of 500 mV in 1 M sodium chloride solution at 45 ºC. The Nyquist plots manifest that at 45 ºC, the specimens with different surface finishes maintain a passive surface because there were only randels-circuit like features in the plots which are ascribed to surface passivation **[16]**. It is also observed that the diameter of the depressed semi-circle, which corresponds to surface inhomogeneity **[17]**, decreased by roughening the surface of specimen. Fig. 10(a) presents the equivalent circuit used for fitting. And the fitting results obtained are listed in Table 5. In this circuit model, R_s stands for solution resistance. According to the results of the table, the values of R_s were similar and can be neglected compared to the charge transfer resistance related to passive film (R_{ct}). As can be seen in Table 5, the values of R_{ct} increased from 23 kΩ·cm^2 to 240 kΩ·cm^2 with a smoother surface. This significant increase of corrosion resistance implies the positive effect of smoother surface on enhancing surface corrosion resistance. Similar results have been obtained from other types of A/F stainless steel **[18]**, rougher surface condition contains a higher density of valleys and ridges on a much larger scale, which are areas for fast oxidation, expected to have a high dissolution rate and in addition, can provide greater specific surface area. As the result of the higher transfer rate and increased amount of charge transfer R_{pass} increases significantly. Constant phase element (CPE) instead of ideal capacitance was utilized in the model for the precise analysis of electrical double layer capacitance, and its impedance expression of CPE is shown as follows **[19]**:

$$Z_{CPE} = P^{-1} \cdot (i\omega)^{-n} \qquad (1)$$

Where *P* is a magnitude parameter, *n* represents the deviation parameter ($0.5 \leq n \leq 1$ is generally measured in equivalent circuit). On this basis, electrical double layer capacitance in the circuit can be calculated using the following equation [20–22]:

$$C_{dl} = P^{1/n} \cdot {R_{ct}}^{(1-n)/n} \qquad (2)$$

The measured values of electrical double layer capacitance are listed in Table 5. The *n* value increased from 0.866 to 0.887 while the surface became smoother, showing the behavior was attributed to surface heterogeneity [20]. The C_{pass} value of 180# was 4.19 × 10^{-5} μF·cm^{-2} and declined to 3.47 × 10^{-5} μF·cm^{-2} when the surface was polished, suggesting an opposite trend of C_{pass} with surface roughness, compared to R_{ct}. According to Helmholtz model of surface film capacitance, the capacitance is in direct proportion to the surface area [21]:

$$C = \frac{\varepsilon_0 \cdot \varepsilon \cdot S}{d} \qquad (3)$$

Where ε_0 is the permittivity of vacuum, ε is the dielectric constant, S is the surface area and d is the thickness of the passive layer. Since ε_0, ε, d were constant in this measurement, the variation of C_{pass} was attributed to the specific surface area changes. The calculation of C_{pass} gave the same indication that a rough surface decreases the surface corrosion resistance of DSS2205 as R_{pass} did.

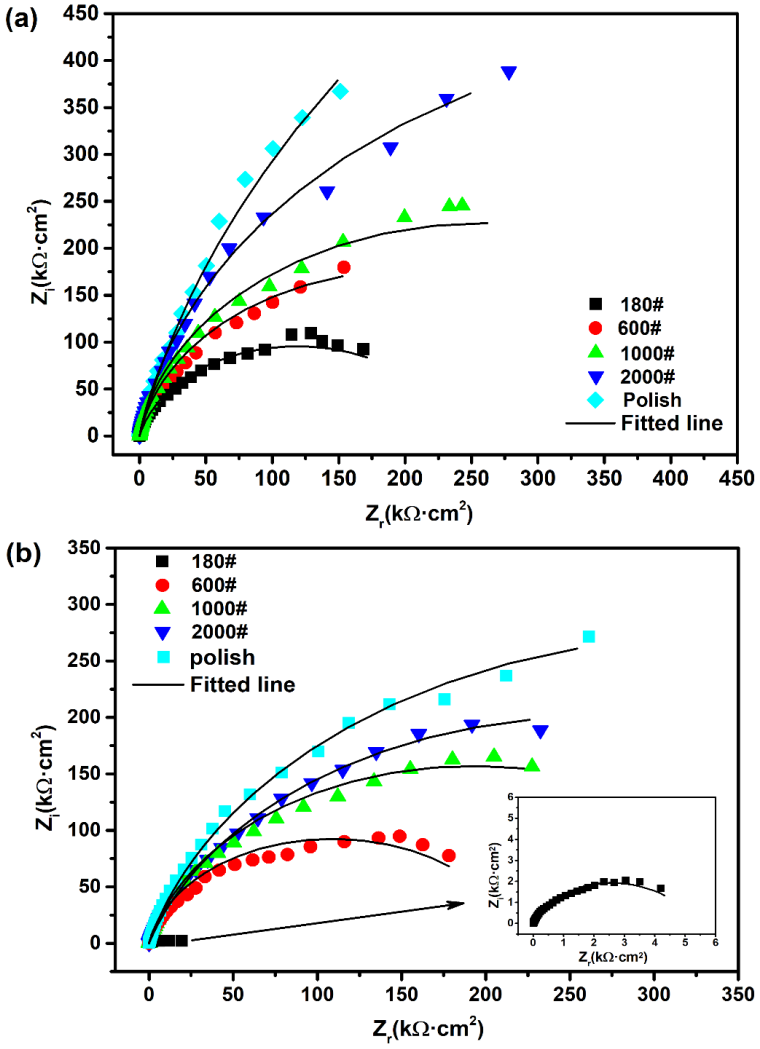

Figure 9. EIS results for DSS2205 with different surface roughness under 500 mV (SCE) in 1 M NaCl at (a) 45 ºC and (b) 50 ºC

Table 5. Results of EIS for DSS2205 with different surface roughness in 1 M NaCl solution on 500 mV (SCE) at 45 ℃

Surface roughness	R_s ($\Omega \cdot cm^2$)	R_{pass} ($\Omega \cdot cm^2$)	CPE_{pass} parameters		C_{pass} ($\mu F \cdot cm^{-2}$)
			P ($\mu F \cdot cm^{-2}$)	n	
180 #	4.21	2.38×10^5	30.8	0.866	41.9
600 #	2.95	3.28×10^5	28.3	0.875	38.9
1000 #	2.98	3.39×10^5	27.9	0.879	38.1
2000 #	2.78	4.41×10^5	27.2	0.882	37.3
Polish to 2.5μm	2.47	1.20×10^6	22.7	0.887	34.7

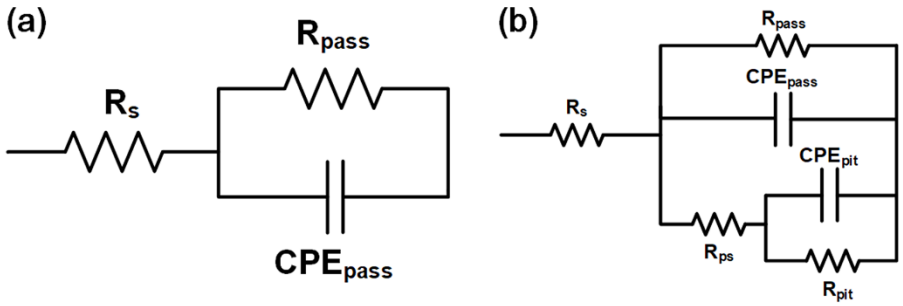

Figure 10. Equivalents circuits used to model the EIS results: (a) passive condition and (b) pitting occurrence

Table 6. Results of EIS for DSS2205 with different surface roughness in 1 M NaCl solution on 500 mV (SCE) at 50 ℃

Surface roughness	R_s ($\Omega \cdot cm^2$)	R_{pass} ($\Omega \cdot cm^2$)	CPE_{pass} parameters		C_{pass} ($\mu F \cdot cm^{-2}$)	R_{ps} ($\Omega \cdot cm^2$)	R_{pit} ($\Omega \cdot cm^2$)	CPE_{pit}		C_{pit} ($\mu F \cdot cm^{-2}$)
			P ($\mu F \cdot cm^{-2}$)	n				P ($\mu F \cdot cm^{-2}$)	n	
180#	2.66	4.90×10^4	193	0.853	28.4×10^{-5}	6.31	3814	103	0.774	78.4
600#	2.57	2.22×10^5	27.1	0.864	35.9×10^{-5}	-	-	-	-	-
1000#	2.51	3.57×10^5	21.8	0.878	29.0×10^{-5}	-	-	-	-	-
2000#	2.64	5.85×10^5	24.2	0.875	14.4×10^{-5}	-	-	-	-	-
Polish to 2.5μm	2.71	7.37×10^5	22.5	0.884	13.2×10^{-5}	-	-	-	-	-

When the temperature increased to 50 ºC, which is above the CPT of 180# ground surface, EIS results are shown in Fig. 9(b). For the specimens with CPT above 50 ºC, the plots were still simple Randles-like features, but a notable decrease had taken place on total impedance for the 180-grit ground sample, implying the occurrence of pitting corrosion. A different equivalent circuit was used to simulate this condition, as shown in Fig. 10(b). R_{ps} represents pitting solution resistance, R_{pit} is the pitting charge transfer resistance and C_{pit} is the pit double layer capacitance. These parallel elements were added to distinguish the pitting area from the passive surface because the anodic current density of the metal surface within the pit led to considerable IR drop, and the parameters are displayed in Table 6. As can be seen from the table, the total impedance of the smoother specimen had reduced by 90-400 $k\Omega \cdot cm^2$ due to the degenerative effect of temperature on the passive film condition and reaction rate [22,23]. The rapid decline of the impedance of the relatively rough 180# surface at 50 ºC was consistent with the results obtained from CPT measurement. In conclusion, the changes of surface impedance revealed the

influence of surface roughness on the surface corrosion behavior of DSS2205 and the generation of stable pitting as the consequence.

3.5. Surface roughness effect on potentiostatic measurement

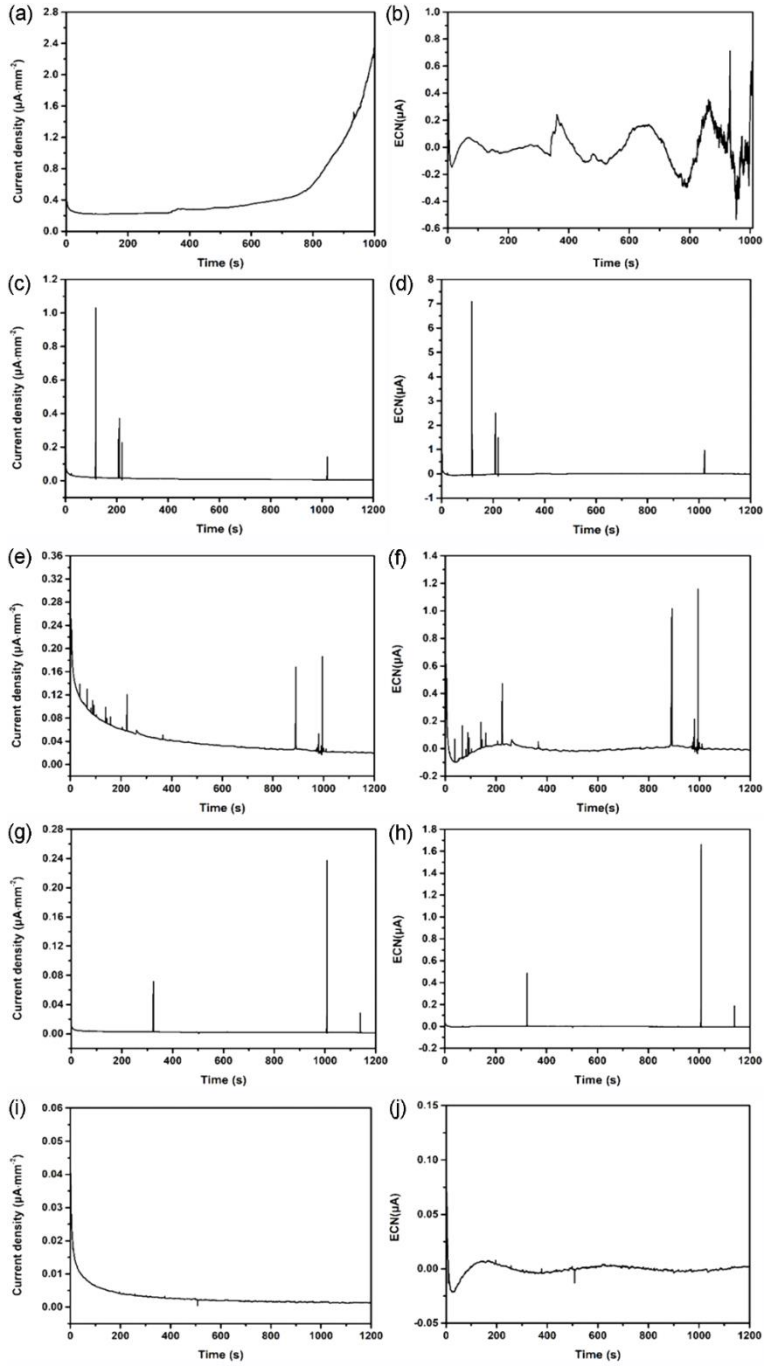

Figure 11. Typical potentiostatic current density curves of different surface roughness DSS2205 samples at 200 mV(SCE) in 1M NaCl at 50 ºC: (a) 180 grit, (c) 600 grit, (e) 1000 grit, (g) 2000 grit, (i) polished; and ECN curve at the same experimental condition: (b) 180 grit, (d) 600 grit, (f) 1000 grit, (g) 2000 grit, (j) polished

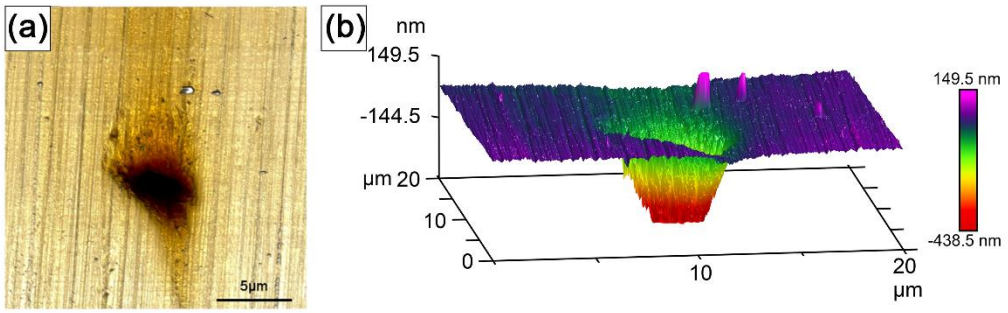

Figure 12. AFM image of the metastable pit obtained in potentiostatic measurement: (a) plane image; (b) three-dimensional image

To further investigate the pitting nucleation behavior shown in the potentiodynamic method, potentiostatic measurement was conducted. The experiment was measured at 45 ºC, 50 ºC, 55 ºC and 60 ºC in light of the polarization curves mentioned above, the applied potential was 200 mV (SCE) in the passive region. Fig. 11 shows the typical potentiosatic curve and the measured electrochemical current noise (ECN) of DSS2205 in 1 M sodium chloride solution. It can be seen that the current density of 180 grit surface finish increased rapidly from less than 300 $nA \cdot mm^{-2}$ to over 2 $\mu A \cdot mm^{-2}$ after anodic polarization for 800 s, implying the tendency for pitting corrosion. In contrast, the current density of the smoother surface maintained at a passive current level of about 100 $nA \cdot mm^{-2}$ and decreased with time. Several current transients were shown in the plot of 600#, 1000#, 2000# surface, however the polished sample exhibited no current peaks. These transients can be described as the propagation and repassivation of metastable pitting [24]. AFM test revealed the dish shape metastable pits on the specimens, as shown in Fig. 12.

In order to quantify the electrochemical activity of the sample surface, the maximum peak current i_m values of specimens at different temperatures are illustrated in Fig. 13. Apparently i_m increased with temperature and was independent of surface roughness. According to the research of Salinas-Bravo and Newman [10], a critical current density of passivation (i_{crit}) exists in the concentrated pit solution. At the temperature below CPT, i_{crit} is lower than the limited diffusion current density, i_{limit}, and the metastable pit is repassivated instead of growing into a stable pit. Therefore, in this measurement, the i_m of metastable pits for all samples were rate-controlling and were close to i_{crit}, which means the pit growth was under charge transfer control and a repassivation process. The standard deviations (SD) of the current transients were also calculated and the results are exhibited in Fig. 14, with each point being repeated three times. The polished sample had the lowest SD at all the conducted temperatures, and in contrast, the 180# surface was prone to metastable pitting with the highest measured SD. It can be concluded that a rougher surface tends to have a wider range of occluded morphology for pit initiation. Additionally, the SD value of polished surface at 60 ºC was still much lower than the SD of 180# at 50 ºC, indicating that the influence of surface roughness on pit initiation is stronger than the temperature factor.

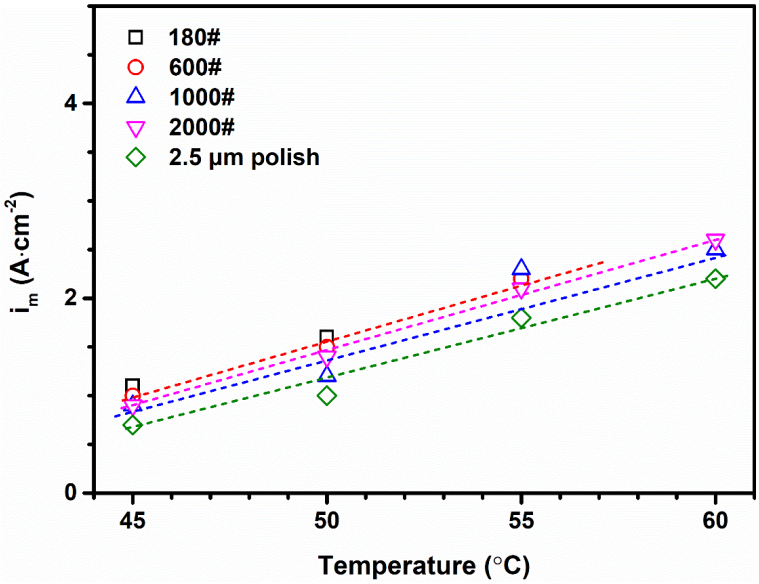

Figure 13. Maximum metastable current density as a function of temperature for DSS2205 with different surface finish in 1M NaCl at 200 mV (SCE)

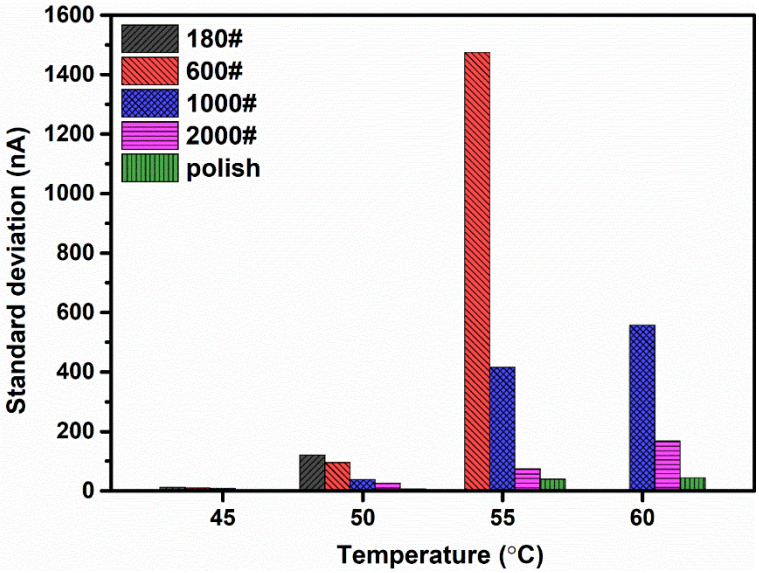

Figure 14. Standard deviation of potentiostatic method for DSS2205 with different surface finish in 1M NaCl at different temperature, 200 mV (SCE)

The metastable pit number per minute based on current transient data is summarized in Fig. 15, with each data point being repeated at least three times. As can be seen from Fig. 15., the metastable pit number per minute was reduced with an improvement of surface roughness. This is because the rough surface has relatively high possibility for the nucleation of metastable pit, since an uneven surface provides much more diffusion-limited areas and various surface defects to maintain the aggressive pit electrolyte [25]. In summary, these results demonstrate that the rougher surface, which contains more confined cavity areas, contributes to the increasing probability of metastable pitting nucleation.

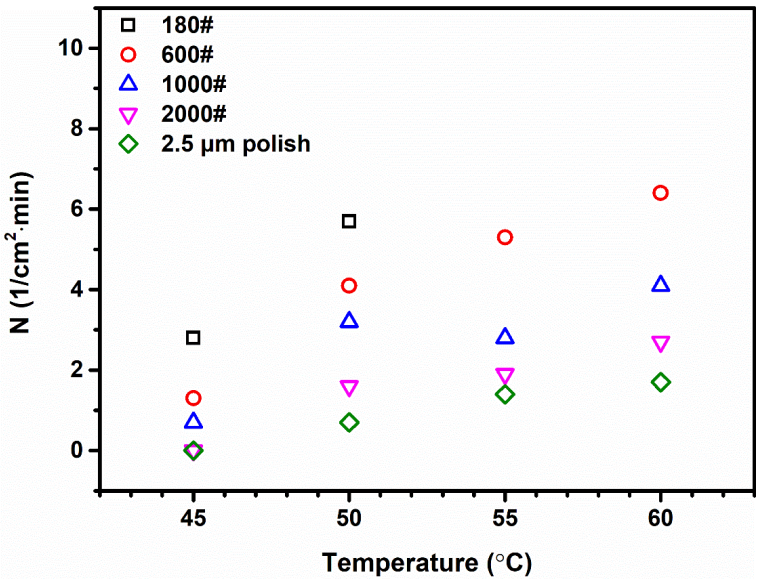

Figure 15. Metastable pit number as a function of temperature for DSS2205 with different surface finish in 1M NaCl at 200 mV (SCE)

3.5. Surface roughness effect on pit morphology and location

Fig. 16 displays the optical microscope image of the pit corrosion attack on the 2205 stainless steel samples obtained from the polarization test. The stable pits on the rough surface were obviously located on the grooves generated by mechanical grinding, suggesting the facilitation of large surface roughness on stable pit occurrence. Specifically, the rough surface provided an occluded area which can maintain the pit's internal solution environment for the pit initiation and the metastable-stable pit transition. Moreover, as can be observed from Fig. 16(c), the stable pit on polished specimen displayed a lacy cover. According to the previous research [26], the formation of perforated lacy cover is due to that the pit chemical environment near the bulk solution cannot reach the critical cation concentration, thus the pit passivates near the mouth, then further dissolutions undercut the passivated parts and holes emerge on the surface, which is observed as lacy cover on metallography. In this work, smooth surface, i.e. the surface of polished specimen, only have shallow cavities and a short diffusion length, so the cations in the pit are easy to diffuse into bulk solution. The lacy cover has formed in this situation and become a barrier to slow the diffusion process and maintain pit growth.

The pit initiation position on duplex stainless steel was investigated in detail with the utilization of Back Scattered Electron Imaging (BSE) on the sample after the potentiostatic test. The images are displayed in Fig. 17. As is shown in Fig. 17, the metastable pits mainly initiated at the austenite-ferrite phase boundary. The reason of this phenomenon is probably ascribed to higher energy at these sites [27]. Some metastable pits can also be observed in the ferrite phase (darker phase), corresponding to the lower pitting resistance equivalent number (PREN) of the ferrite phase [28]. In addition, the position of metastable pits on the different surface roughness samples was similar, so it can be deduced that the influences of surface roughness on both phases of duplex stainless steel are equal, and the distribution of metastable pits initiation sites is not affected by surface roughness.

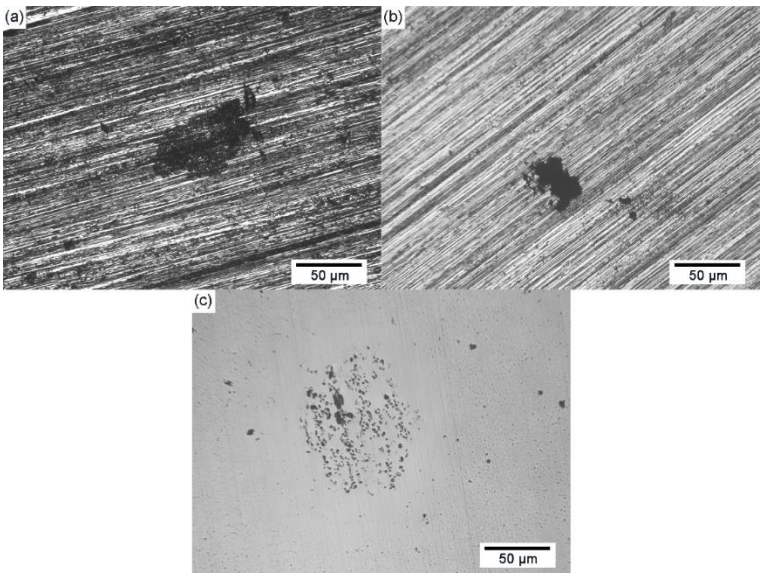

Figure 16. Optical microscope image of the stable pit on 2205 samples after polarization test: (a) 180#; (b) 1000#; (c) polished

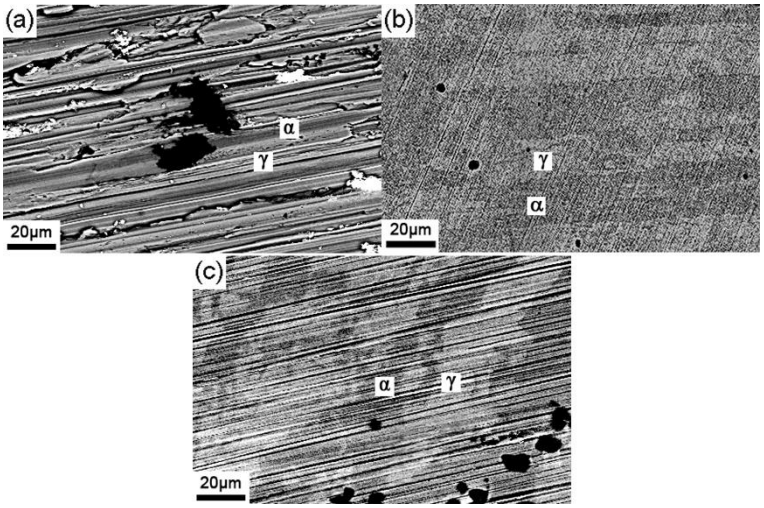

Figure 17. BSE images of 2205 samples after potentiostatic test: (a) 180#; (b) 1000#; (c) polished. α and γ represent the ferrite phase and austenite phase in the images separately

3.6. Relationship between surface roughness parameters and pitting corrosion

The data obtained from the method above suggests a strong impact of surface roughness on the nucleation of the metastable pit and its transition to stable pit. To better describe this effect, a specific surface roughness parameter should be introduced to establish the quantitative relationship. The main parameters to characterize surface roughness are arithmetical mean roughness (Ra) and maximum height roughness (Rz). But these parameters do not have an explicit correlation with the usual pit parameters. For the purpose of providing an accurate description of effective depth for various surface conditions, the depth-width ratio of the groove was calculated in present work. In order to insure the statistical accuracy of the depth-width ratio, the 12 deepest grooves, which were mainly located at austenite-ferrite

phase boundary, were measured on each surface finish. For a specific groove, the distance between both ends of the open mouth was calculated as the width *w*, and the length between pit mouth and the bottom can be defined as the depth *d*. A schematic of the computed model is shown in Fig. 18. The statistical results of the width and depth are summarized in Table 7. As can be seen from the table, the average value and standard deviation for the depth of the grooves increased while surface became rougher, but the change of depth is obviously larger than the change of width, suggesting that the open angles of the grooves on the different surface conditions varied significantly [29]. Fig. 19 exhibited the distribution of depth-width ratios for different surface roughness. It can be seen from the plot that all the distributions of the depth-width ratios accorded with the C. Hence, the mean value can be used to characterize the ratio of different surface roughness, in other words, the average depth-width ratio value can represent the openness of pre-existent pit areas on different surface conditions. Both the mean value and the standard deviation of the depth-width ratio increased with the enhancement of surface roughness, which indicates a positive correlation between depth-width ratio and effective diffusion length in agreement with the Salinas-Bravo and Newman model [10].

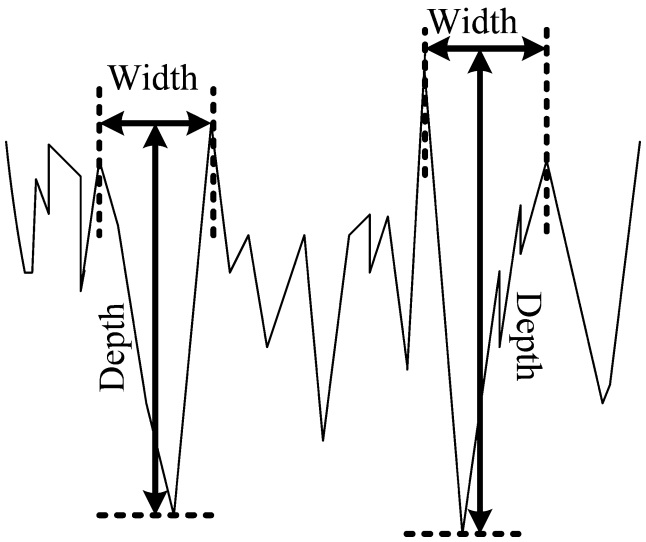

Figure 18. Schematic of the measurement for depth-width ratio

Table 7. Average value and standard deviation of depth and width for different surface finish of DSS2205

Surface roughness	Average width (μm)	SD of width (μm)	Average depth (μm)	SD of depth (μm)
180#	9.251	5.351	1.524	0.818
600#	2.033	1.348	0.223	0.160
1000#	1.904	0.846	0.077	0.021
2000#	1.798	0.695	0.024	0.011
2.5μm polished	1.325	0.216	0.021	0.007

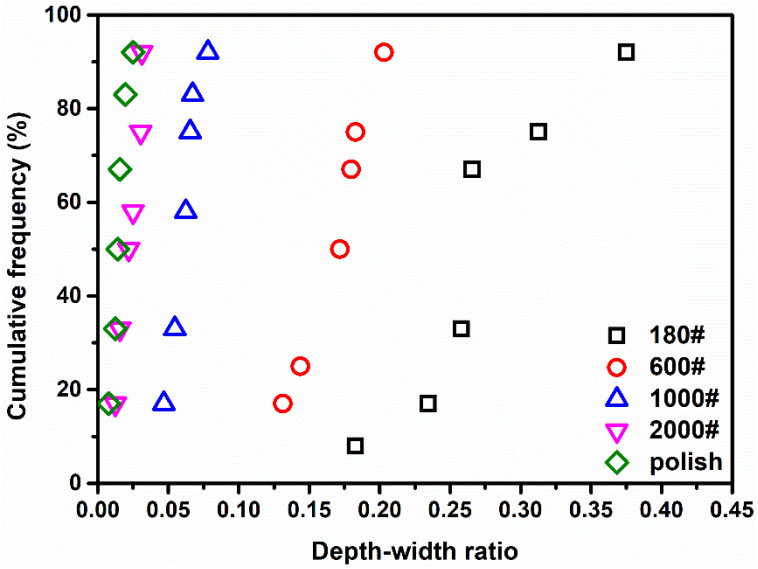

Figure 19. The distribution of depth-width ratios for different surface roughness of DSS2205

According to previous research, the anodic salt film was assumed to be formed to maintain the inner saturated concentration, initiate the metastable pit and sustain the stable pit [6]. It was described as an extremely thin film and thought to be formed due to the chemical equilibrium between the ionic solution and solid metal [30,31], so the ion concentration in the pit solution beneath the salt film was thought to be constantly close to saturation. This sufficient concentration of metal ions was considered to be the essential condition for the allowance of pit growth and the metastable-to-stable transition [32,33]. Furthermore, within the pitting process, the migration effect on the transport of reactive ions can be neglected due to the assumption that the bulk solution acts as the supporting electrolyte [34]. In the light of these theories, the total ionic flux can be calculated by Fick's first law based on the simplified one-dimensional linear diffusion model, using the following equation:

$$total\ flux = D \cdot \frac{C_0}{r} \cdot L \qquad (4)$$

Where D is the diffusion coefficient, C_0 is the concentration of the pit bottom which beneath the salt film, L is the length of the grooves, and r is the depth-width ratio, which is defined to be:

$$r = \frac{d}{w} \qquad (5)$$

Assuming that the interfaces between the pit domain and the bulk solution of different surface conditions have equal area, the limited diffusion current density i_{limit} can be obtained with the insertion of Faraday's law into equation (5), and may be written as:

$$i_{limit} = \frac{nFDC_0}{r \cdot S_0} \qquad (6)$$

Where F is Faraday constant, n is the valence number of ions, S_0 is the critical area of interface. Obviously, i_{limit} is inversely proportional to the depth-width ratio, and this correlation is similar to the relation between effective diffusion length and anodic diffusion current density in the hemisphere pit model, which was summarized by other researchers in the following equation [35]:

$$i = \frac{nFDC_{sat}}{h_{\text{eff}}} \qquad (7)$$

Where D is diffusion coefficient, C_{sat} is the critical metal ions concentration, F is Faraday constant, h_{eff} is the effective diffusion length. On account of the small change of the measured solution temperatures, D and C_{sat} can be considered as unchanged in this situation. Based on the above comprehension, the effective diffusion length can be broadly understood as the length of the pit when pit open zone reaches the critical size, which is corresponding to the depth-width ratio in this research.

Fig. 20(a) shows the change tendency of i_{limt} with the reciprocal of depth-width ratio. In the CPT transition model [10,36,37], i_{crit} is equal to i_{limit} at CPT. Also, the functional relation of i_{crit}-temperature corresponds to that of maximum transient current i_m with temperature, according to the analysis of potentiostatic measurement in Fig. 15, so i_{limit} values for different surface roughness conditions can be estimated at their corresponding CPT. Fig. 20(a) illustrates that there is a negative linear correlation between i_{limt} and the reciprocal of depth-width ratio, indicating the depth-width ratio and h_{eff} have a similar functional relationship with the anodic diffusion current density. Hence, the strong correlation between aspect ratio and h_{eff} can be seen, and as a result, the aforementioned understanding of depth-width ratio and its effectiveness as a quantitative parameter to represent the diffusion length for different surface roughness has been proved.

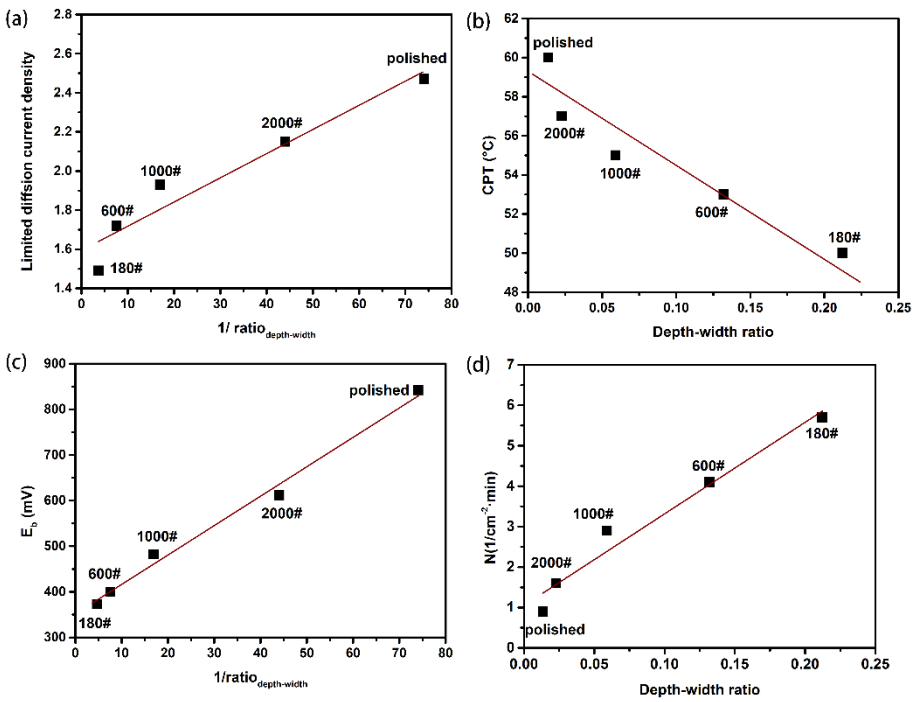

Figure 20. Pit corrosion parameters as a function of the depth-width ratio for the different surface roughness samples of DSS2205: (a) limited diffusion current density; (b) CPT; (c) pitting potential; (d) metastable pit numbers

Fig. 20(b) shows the relationship between the CPT of DSS2205 stainless steel and depth-width ratio for different surface roughness. It can be seen from Fig. 20(b) that good linearity between CPT and depth-width ratio was achieved, which is consistent with Salinas-Bravo and Newman model. The increase of limited diffusion current i_{limt} was attributed to the decrease of diffusion length which has the strong correlation with the change of surface cavity openness.

The interrelation between pitting potential E_b of DSS2205 stainless steel and depth-width ratio above CPT temperature is displayed in Fig. 20(c). It is observed that E_b dropped linearly as the reciprocal of width-depth ratio decreased. This correlation reflects the effectiveness of depth-width ratio for estimating pitting corrosion susceptibility. Rougher surface provides much more occluded geometries, leading to the increase of effective diffusion length and decline of i_{limit}. Due to the linear dependence of pitting potential on the logarithm of i_{limit} [38], E_b decreased as the result of the drop of i_{limt}.

Additionally, the correlation between metastable pit numbers and the depth-width ratio of the specimens is shown in Fig. 20(d). It is clear that the pit initiation probability increased linearly with the increase of width-depth ratio. Hence, the pit initiation stage is also affected by effective diffusion length and the electrochemistry in the primary sites, which needs further investigation in the future.

Given these functional relationships between depth-width ratio and pitting characteristic parameters, depth-width ratio is significantly accurate to represent pitting corrosion susceptibility as a quantitative surface roughness parameter.

4. CONCLUSIONS

The pitting corrosion of different surface roughness for DSS2205 stainless steel has been studied by a series of electrochemical measurements. The pitting corrosion resistance of DSS2205 was distinctly influenced by surface finish condition. Compared with rougher surface, smoother surface condition led to a better pitting resistance and a lower susceptibility. The novelty of this research is in introducing depth-width ratio as an effective parameter to represent the relationship between surface roughness and pitting corrosion parameters. The conclusions obtained from this research can be summarized as：

⑴ With the surface becoming rougher, the CPT value and E_b of DSS 2205 stainless steel decline, indicating that rough surface generates more occluded sites which is apt to maintain the pit propagation process and facilitate metastable-stable transition;

⑵ Due to the area effect caused by surface roughness, the corrosion resistance of DSS 2205 stainless steel is lower on rougher surface, thus the possibility of pitting corrosion increased.

⑶ The number of metastable pits on DSS 2205 stainless steel increased as the surface became rougher. This result demonstrates that rough surface finish contributed to the increase of pitting initiation and hence raises the possibility of both metastable and stable pitting for the material.

⑷ The metastable pits of different surface roughness specimens are mainly located at the ferrite-austenite phase boundary, so the distribution of pits on the metallographic structure is not discernibly affected by the surface roughness factor.

⑸ Depth-width ratio of the surface occluded site is an effective characterization parameter of the surface roughness and could accurately represent the effective diffusion length of the pit, according to calculations. Consequently, it is suggested that the relationship between surface roughness and pitting corrosion susceptibility can be characterized by this aspect ratio with i_{limit}, CPT, E_b and the pit initiation rate.

ACKNOWLEDGEMENTS
This research is supported by National Key Research and Development Program of China (No. 2018YFB0704400) and National Nature Science Foundations of China (Grant No. 51671059). Chen Yan from Research Center for Analysis and Measurement, Fudan University is appreciated for the great help of AFM analysis with Dimension Icon AFM (Bruker, Santa Barbara, CA).

References

1. K. Sasaki and G.T. Burstein, *Corros. Sci.*, 38 (1996) 2111.
2. M.H. Moayed, N.J. Laycock, and R.C. Newman, *Corros. Sci.*, 45 (2003) 1203.
3. T. Mathiesen, T.S. Nielsen, J.E. Frantsen, J. Kold and A.R. Boye-Moeller, Influence of Various Surface Conditions on Pitting Corrosion - Resistance of Stainless Steel Tubes Type EN1.4404, CORROSION 2006, San Diego, USA, 2006, 6095.
4. T. Hong and M. Nagumo, *Corros. Sci.*, 39 (1997) 1665.
5. Y. Zuo, H. Wang and J. Xiong, *Corros. Sci.*, 44 (2002) 25.
6. N.J. Laycock, M.H. Moayed and R.C. Newman, *J. Electrochem. Soc.*, 145 (1998) 2622.
7. A. Burkert, K. Schilling and A. Heyn, *Mater. Corros.*, 55 (2004) 787.
8. H.S. Klapper, A. Burkert, A. Burkert, J. Lehmann and A.L. Villalba, *Corrosion*, 67 (2011) 075004.
9. G.S. Frankel, *J. Electrochem. Soc.*, 145 (1998) 13.
10. V.M. Salinas-Bravo and R.C. Newman, *Corros. Sci.*, 36 (1994) 67.
11. B. Deng, Y.M. Jiang, J. Gong, C. Zhong, J. Gao and J. Li, *Electrochim. Acta*, 53 (2008) 5220.
12. X. Wu, Y.Y. Yang, Y.T. Sun, Y.Y. Liu, J. Li, Y.M. Jiang, *Corros. Sci.*, 149 (2019) 29.
13. R. Ovarfort, *Corros. Sci.*, 29 (1989) 987.
14. G.T. Burstein and S.P. Vines, *J. Electrochem. Soc.*, 148 (2001) B504.
15. A. Igual Muñoz, J. García Antón, J.L. Guiñón and V. Pérez Herranz, *Corros. Sci.*, 49 (2007) 3200.
16. A. Leon and E. Aghion, *Mater. Charact.*, 131 (2017) 188.
17. V. Feliu, J.A. González, C. Andrade and S. Feliu, *Corros. Sci.*, 40 (1998) 975.
18. D. Wallinder, J. Pan, C. Leygraf and A. Delblanc-Bauer, *Corros. Sci.*, 41 (1998) 275.
19. N.S. Ayati, S. Khandandel, M. Momeni, M.H. Moayed, A. Davoodi and M. Rahimizadeh, *Mater. Chem. Phys.*, 126 (2011) 873.
20. B. Hirschorn, M.E. Orazem, B.T ribollet, V. Vivier, I. Frateur and M. Musiani, *Electrochim. Acta*, 55 (2010) 6218.
21. N. Ebrahimi, M. Momeni, A. Kosari, M. Zakeri and M.H. Moayed, *Corros. Sci.*, 59 (2012) 96.
22. M. Hoseinpoor, M. Momeni, M.H. Moayed, A. Davoodi, *Corros. Sci.*, 80 (2014) 197.
23. D.D. Macdonald, *J. Electrochem. Soc.*, 139 (1992) 3434.
24. H.S. Klapper, J. Goellner, A. Burkert, A. Heyn, *Corros. Sci.*, 75 (2013) 239.
25. M.H. Moayed and R.C. Newman, *Mater. Corros.*, 56 (2005) 166.
26. P. Ernst, N.J. Laycock, M.H. Moayed and R.C. Newman, *Corros. Sci.*, 39 (1997) 1133.
27. H. Luo, C.F. Dong, X.G. Li and K. Xiao, *Electrochim. Acta*, 64 (2012) 211.
28. M. Gholami, M. Hoseinpoor and M.H. Moayed, *Corros. Sci.*, 94 (2015) 156.
29. W.M. Tian, B.X. Chao, X.Y. Xiong, Z.Y. Li, *Int J Electrochem Sci.*, 13 (2018) 3107.
30. J.W. Tester, *J. Electrochem. Soc.*, 122 (1975) 1438.
31. S. Scheiner and C. Hellmich, *Corros. Sci.*, 49 (2007) 319.
32. R.C. Newman and M.A.A. Ajjawi, *Corros. Sci.*, 26 (1986) 1057.
33. Pistorius, P.C. and Burstein, G.T., *Philos. Trans. R. Soc., A*, 341 (1992) 531.
34. J.R. Galvele, *J. Electrochem. Soc.*,123 (1976) 11.
35. G.T. Gaudet, W.T. Mo, T.A. Hatton, J.W. Tester, J. Tilly, H.S. Isaacs and R.C. Newman, *AIChE J.*, 32 (1986) 949.
36. T.S. Li, J.R. Scully and G.S. Frankel, *J. Electrochem. Soc.*, 165 (2018) C484.

37. T.S. Li, J.R. Scully and G.S. Frankel, *J. Electrochem. Soc.*, 165 (2018) C762.
38. N.J. Laycock and R.C. Newman, *Corros. Sci.*, 39 (1997) 1771.